JOURNAL OF COMPUTATIONAL PHYSICS **131,** 354–367 (1997)
ARTICLE NO. CP965606

On the Numerical Solution of the Sine–Gordon Equation

II. Performance of Numerical Schemes

M. J. Ablowitz,* B. M. Herbst,† and C. M. Schober‡

*Program in Applied Mathematics, University of Colorado, Boulder, Colorado 80309; †Department of Mathematics and Applied Mathematics, University of Cape Town, Private Bag, Rondebosch 7700, South Africa; ‡Department of Mathematics, Old Dominion University, Norfolk, Virginia 23529-0077
E-mail: schober@math.odu.edu.

Received January 3, 1996; revised October 17, 1996

The phase space of sine–Gordon possesses tori and homoclinic structures. It is important to determine how these structures are preserved by numerical schemes. In this, the second of two papers on the numerical solution of the sine–Gordon equation, we use the nonlinear spectrum as a basis for comparing the effectiveness of symplectic and nonsymplectic integrators in capturing infinite dimensional phase space dynamics. In particular, we examine how the preservation of the nonlinear spectrum (i.e., the integrable structure) depends on the order of the accuracy and the symplectic property of the numerical scheme.

1. INTRODUCTION

In a previous study of the sine–Gordon equation,

$$u_{tt} - u_{xx} + \sin u = 0 \tag{1}$$

with periodic boundary conditions, $u(x, t) = u(x + L, t)$, we investigated how the presence of homoclinic structures affects numerical solutions of the sine–Gordon equation. We concentrated our efforts on the doubly discrete, completely integrable discretization due to Hirota. Since it shares many of the essential properties of the sine-Gordon equation, including integrability, it seems reasonable to expect that it should be eminently suitable as a numerical scheme. One certainly does not expect it to become unstable. Yet, this is exactly what happens if initial values are chosen in certain regions of phase space [3].

On the other hand, in [10] we observed that a *first* order symplectic scheme remains well-behaved using the same initial values. Higher order symplectic schemes did become unstable, but still appeared to be better behaved than nonsymplectic schemes. This may be a significant observation—since symplectic schemes are designed to preserve the geometric properties of Hamiltonian systems exactly—one has reason to expect that they should perform qualitatively better than nonsymplectic schemes. This is the case in low dimensional systems and in Section 1 we explain in detail why the symplectic property is so important for *planar* Hamiltonian systems. The question is whether this superior behavior carries over to high-dimensional systems, as our earlier experiments with symplectic integrators of the sine–Gordon equation might indicate. In this paper we set out to answer this question.

In order to determine the effectiveness of symplectic integrators, it is very useful to have a simple description of the geometry of phase space which can be used to determine how well the numerical schemes preserve the phase space structure. Fortunately, such a description based upon the spectrum of the associated linear eigenvalue problem is developed in [7]. In this description, the geometry of phase space is represented by the discrete eigenvalues of an associated eigenvalue problem. In particular, sensitive regions are described by the ''unstable'' double points in the spectrum. The spectrum is not only useful to understand the nature of the instabilities observed in many numerical discretizations of the sine–Gordon equation, it also provides a description of the qualitative properties of the numerical schemes themselves. In fact, the spectrum enables one to *define* the qualitative properties of the numerical schemes and it provides a quantitative measure of these properties. Thus we are in a position to compare the qualitative properties of different numerical schemes in a quantitative way. We are particularly interested in a comparison between symplectic and nonsymplectic schemes for high, but finite, dimensional Hamiltonian systems.

In particular, in this paper we address the following questions:

- Do symplectic integrators preserve the structure of the sine–Gordon phase space appreciably better than nonsymplectic methods? More specifically, do trajectories explore a smaller region of phase space when symplectic methods are used?
- Does the relative performance of symplectic integrators improve if one chooses initial values away from

0021-9991/97 $25.00

the unstable homoclinic manifolds? If very long time integrations are considered?

• How important is the order of accuracy of the numerical scheme in the preservation of the qualitative properties of the phase space?

It is important to note the following:

• We compare the *qualitative* properties of several symplectic schemes and nonsymplectic schemes of the same order. For example, we have not attempted to optimize the nonsymplectic schemes by adjusting the order or the time step. This could lead to major improvements of the nonsymplectic Runge–Kutta schemes that we use. Incidentally, symplectic schemes do not benefit in general from adjusting the time step, see Sanz-Serna and Calvo [17].

• We obtain the finite dimensional Hamiltonian system from a finite difference and Fourier spectral spatial discretization of the sine–Gordon equation. The resulting Hamiltonian systems turn out to be separable—a situation that is particularly advantageous for symplectic schemes since separability allows the construction of *explicit* symplectic schemes.

It should be clear that we have chosen circumstances that are particularly favorable towards the use of symplectic schemes. The symplectic schemes are implemented in a particularly efficient manner and they are compared with far from optimal nonsymplectic schemes. Even so, we find very little difference in the performance of the symplectic and nonsymplectic schemes. Unlike the situation for planar systems, the ability of the numerical schemes to preserve the phase space structure of high-dimensional Hamiltonian systems appears to depend more upon the accuracy of the scheme rather than the property of symplecticness.

Although we have by no means tested all available symplectic schemes, we believe that our results do reflect the importance, or lack thereof, of the preservation of symplecticness in the integration of the high-dimensional Hamiltonian systems which result from the semidiscretization of the infinite dimensional systems of soliton theory.

2. PLANAR HAMILTONIAN SYSTEMS

Using the coordinates (p, q), two-dimensional Hamiltonian systems can be written as

$$\frac{dp}{dt} = -\frac{\partial H}{\partial q}, \frac{dq}{dt} = \frac{\partial H}{\partial p}, \tag{2}$$

where the Hamiltonian H is well-behaved, typically an analytical function of p, q. The system (2) has two important properties: The Hamiltonian is a constant of motion and the phase flow preserves area. The former property means that the system is *integrable* and the second is a fundamental geometric property of planar Hamiltonian systems—it holds *only* for Hamiltonian systems; see, e.g., [5]. It is our purpose to discretize (2), retaining as much of these two properties as possible.

It turns out that consistent discretizations in general are not able to preserve both the area as well as the Hamiltonian. Since area preservation (in particular its higher dimensional analogue) is the more fundamental of the two properties, much effort has gone onto the construction of the so-called *symplectic* discretizations. Here symplectic simply means a consistent, area preserving discretizations of (2); see, e.g., [17] for a comprehensive overview.

It is quite straightforward to verify that a map is area preserving in practice. Let

$$(P, Q) = \phi(p, q) \tag{3}$$

define a smooth transformation in some domain Ω. According to the standard rules for changing variables in an integral, this transformation preserves area if and only if its Jacobian is identically one, i.e.,

$$\frac{\partial P}{\partial p}\frac{\partial Q}{\partial q} - \frac{\partial P}{\partial q}\frac{\partial Q}{\partial p} = 1 \quad \forall (p, q) \in \Omega. \tag{4}$$

Let us now simplify even more and assume that the Hamiltonian is separable; i.e., one can write $H(p, q) = T(p) + V(q)$. The following is a first-order discretization of (2),

$$\begin{aligned} p_{n+1} &= p_n - kV'(q_n) \\ q_{n+1} &= q_n + kT'(p_{n+1}), \end{aligned} \tag{5}$$

where a prime denotes a derivative with respect to the argument and k is the time step. To check that the transformation $(p_n, q_n) \to (p_{n+1}, q_{n+1})$ is symplectic, one simply checks that its Jacobian equals one. Also note that it is *explicit,* which is a consequence of the separability of the Hamiltonian. Although (5) is only first order there are several procedures to construct higher order symplectic schemes. Still assuming that the Hamiltonian is separable, a general form of higher order schemes may be given by, e.g., [19],

$$\begin{aligned} p_{i+1} &= p_i - C_i kV'(q_i) \\ q_{i+1} &= q_i + D_i kT'(p_{i+1}), \end{aligned} \tag{6}$$

where $i = 1, \ldots, m$ and the coefficients C_i and D_i are determined in order for the scheme to be symplectic and of $O(k^m)$. Here p_1 and q_1 are the numerical approximation

at the time t and p_{m+1} and q_{m+1} are the approximations at the next time level, $t + k$. For example, the first-order scheme (5) is given by $m = 1$ and

$$C_1 = 1, \quad D_1 = 1.$$

Similarly a second-order scheme is given by $m = 2$ and

$$C_1 = 0, \quad C_2 = 1, \quad D_1 = \tfrac{1}{2} = D_2.$$

Note that the schemes defined by (6) are explicit since the Hamiltonian is separable. We should also point out that this is only one way of constructing higher order symplectic discretizations and the one used in this study; for an explanation of other possibilities the reader is referred to [17].

As alluded to above, symplectic discretizations lose the integrability of the continuous planar Hamiltonian systems. Moreover, a simple geometric argument shows that symplectic schemes, in general, are *chaotic,* regardless of the size of the time step k or the order of the discretization (see [12] for a more detailed discussion). In this sense symplectic discretizations of planar Hamiltonian systems tend to be nonlinearly unconditionally unstable. But what does this mean in practice, is it important numerically?

As an example, let us consider the pendulum equation,

$$q'' + \sin q = 0, \tag{7}$$

which can be written as the Hamiltonian system,

$$\begin{aligned} q' &= p \\ p' &= -\sin q, \end{aligned} \tag{8}$$

with the Hamiltonian function given by

$$H(q, p) = \tfrac{1}{2}p^2 - \cos q. \tag{9}$$

It is straightforward to establish that there is a homoclinic orbit to the fixed point at $(p, q) = (0, \pi)$ given by

$$\tfrac{1}{2}p^2 - \cos q = 1,$$

or explicitly written as

$$q(t) = \pi + 4 \arctan[\exp(t + \gamma)]. \tag{10}$$

Note that the phase space is a cylinder; i.e., we identify the lines $(p, -\pi)$ and (p, π) in the phase plane (p, q) as usual.

Figure 1a shows the situation if the pendulum equation is solved using the first-order symplectic scheme (5) with a time step $k = 0.2$. Apparently all is well; no abnormal behavior is observed. However, if a small region about the fixed point at the origin is magnified as in Fig. 1b (note the change in scale from Fig. 1a), the situation changes considerably. Now the familiar KAM features—chaotic regions, resonant islands, and invariant curves—become visible. These features depend only on the area preserving

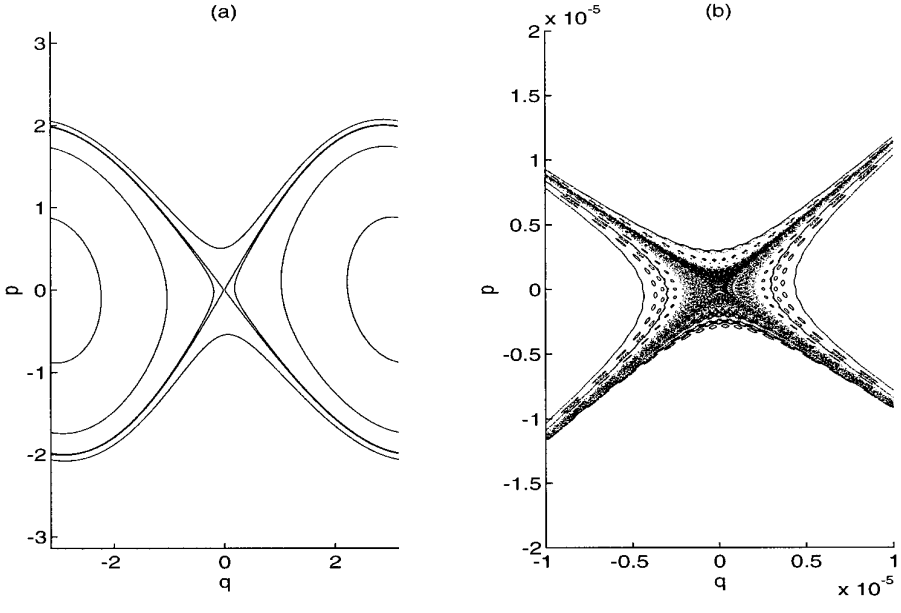

FIG. 1. The solution of the pendulum equation; (b) is a closeup view of (a).

property of the discretization; for example, the situation does not improve if one uses a higher order symplectic discretization. Even so, the situation is not nearly as bad as it might appear. Accordingly, we now proceed to measure the extent of the chaotic presence relative to the discretization parameter.

In the first series of experiments the distance to the first invariant curve is measured, as one moves away from the fixed point at π (homoclinic orbit).[1] This splitting distance D is measured as a function of k for first-, fourth-, and eight-order symplectic schemes of the form (6), denoted by SI1, SI4, and SI8, respectively. The results are shown in Fig. 2.

The graphs indicate an exponential decay of the chaotic region around the separatrix, as a function of k. Thus, assuming that the splitting distance D depends on the time step k as

$$D \propto \exp(-\alpha/k),$$

one can measure α for the different experiments shown in Fig. 2. The results are given in Table I.

Table I shows that the rate of decay does not depend on the *order* of the discretization. In fact, this can be justified analytically in a nonrigorous manner using Mel'nikov's method (see [12]); more rigorous arguments have been given by [16, 14, 15], among others.

In the second set of experiments we measure the *lobe area,* A, between the stable and unstable manifolds. The situation is illustrated in Fig. 3 which was obtained by iterating a small section of the *linear* stable and unstable manifolds at the origin backwards and forwards, respectively. We measure the area of one of the small lobes enclosed between the stable and unstable manifolds. Note that all the lobes have the same area—symplectic integrators are, after all, designed to preserve area. Without going into any details (but see [12]), we note that the lobe area is easily calculated if two consecutive intersection points are known, by invoking the Mackay–Meiss–Percival action principle.

TABLE I

Decay-Rate Obtained from Varying k

Integrator	α
SI 1	4.6
SI 4	4.3
SI 8	4.4

Measuring the lobe area as a function of the time step k for the first-order symplectic scheme (5), the results are shown in Fig. 4.

Again assuming a relationship between the lobe area A and the time step of the form

$$A \propto \exp(-\alpha/k),$$

the average value of α is given by 8.95. It is no accident that this value turns out to be about twice as big as the value for Fig. 2. In fact, from theoretical considerations (see [12]), we expect $\alpha = \pi^2/2$ in the case of Fig. 4 and $\alpha = \pi^2$ in the case of Fig. 2.

In summary, for planar Hamiltonian systems, symplectic

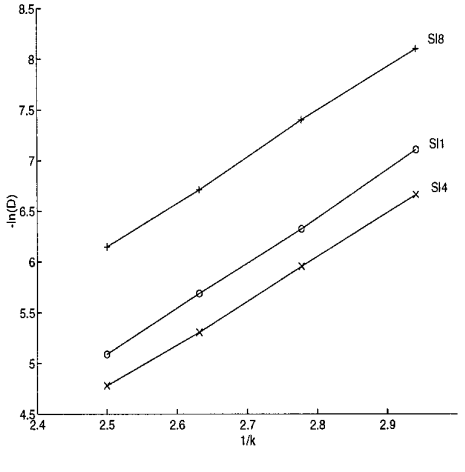

FIG. 2. Exponential decay of the chaotic region as k is decreased, for SI1, SI4, and SI8.

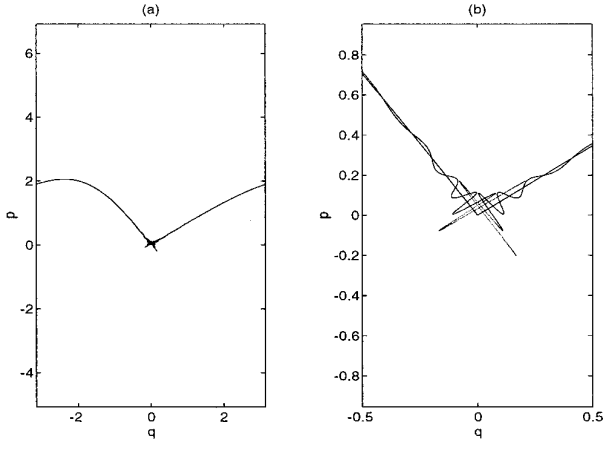

FIG. 3. Homoclinic tangles in the numerical solution of Duffing's equation obtained from the first-order SI.

[1] This corresponds to what is usually referred to in dynamical systems as the *last* invariant curve.

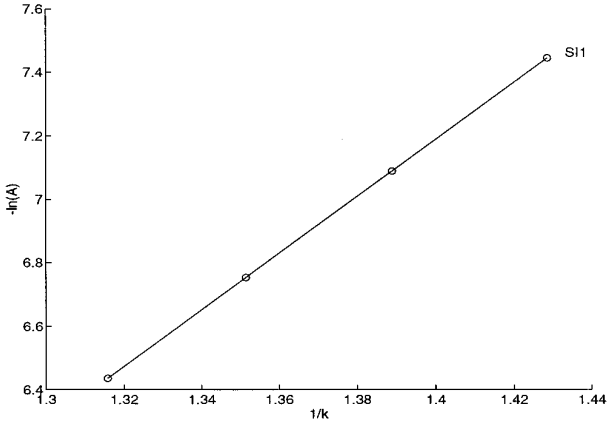

FIG. 4. Exponential decay in the size of the area enclosed between the stable and unstable manifolds, as a function of k.

integrators have the remarkable property that they preserve the integrability of the continuous system with exponential accuracy. More detailed theoretical investigations show that this is a direct consequence of the area preserving property of the symplectic schemes; *it is not necessarily shared by nonsymplectic schemes.* Moreover, all symplectic schemes, regardless of their order, preserve the integrability with the similar accuracy. Thus there is no need to use anything higher than a first-order scheme if one is only interested in preserving the integrability of the planar system. However, there is seldom any serious interest in solving planar Hamiltonian systems numerically. Evidence that the situation may not be quite as straightforward for higher dimensional systems is already provided by Sanz-Serna and Calvo [17]. They find that different symplectic schemes may behave very differently which is a clear indication that it is not only the symplectic property that is important as we find in the case of planar systems. In order to find out how well symplectic schemes preserve the qualitative properties of higher dimensional systems, we turn to the infinite dimensional sine–Gordon equation.

First we shall briefly mention a few of the special properties of the sine–Gordon equation.

3. INTEGRABLE STRUCTURE OF THE SINE–GORDON EQUATION

The sine–Gordon equation can be viewed as an infinite dimensional Hamiltonian system,

$$q_t = \frac{\delta H}{\delta p}, p_t = -\frac{\delta H}{\delta q} \tag{11}$$

with

$$H(p,q) = \int_0^L [\tfrac{1}{2}p^2 + \tfrac{1}{2}(q_x)^2 + 1 - \cos q]\, dx \tag{12}$$

and where $q := u$ and $p := u_t$ are the conjugate variables and δ denotes the variational derivative.

The Poisson bracket of any two functionals F and G is defined to be

$$\{F, G\} = \int_0^L \left[\frac{\delta F}{\delta q}\frac{\delta G}{\delta p} - \frac{\delta F}{\delta p}\frac{\delta G}{\delta q}\right] dx, \tag{13}$$

and the evolution of any functional F under the sine–Gordon flow is governed by

$$\frac{dF}{dt} = \{F, H\}. \tag{14}$$

Obviously, the Hamiltonian H is conserved by the sine–Gordon flow. Moreover, the sine–Gordon equation is a completely integrable system as there exists an infinite family of conserved functionals in involution with respect to the Poisson bracket (13). This allows the sine–Gordon equation to be solved with the inverse scattering transform.

In general the integrability is lost by numerical discretizations (a notable exception is the double discrete, completely integrable discretization due to Hirota, discussed in more detail in [3]). In the case of infinite-dimensional problems, this may have severe adverse effects on the quality of the numerical solutions, in particular in the vicinity of sensitive structures such as homoclinic orbits. However, it is not obvious how to determine the proximity to homoclinic manifolds from the global constants of motion; another representation is called for. We now proceed to show how the geometric structure of the infinite-dimensional phase space may be described in terms of the Floquet discriminant. More specifically, it implicitly defines the homoclinic orbits and allows one to measure the width of the chaotic layer which appears about the homoclinic orbits when the system is perturbed.

3.1. *Spectral Theory*

The phase space of the sine–Gordon equation with periodic boundary conditions can be described in terms of the spectrum of the linear operator (the spatial part of the associated Lax pair; for a detailed description see [7])

$$\mathscr{L}(\boldsymbol{u}, \lambda) = \left[A\frac{d}{dx} + \frac{i}{4}B(u_x + u_t) + \frac{1}{16\lambda}C - \lambda I\right], \tag{15}$$

where

$$A = \begin{pmatrix} 0 & -1 \\ 1 & 0 \end{pmatrix}, \quad B = \begin{pmatrix} 0 & 1 \\ 1 & 0 \end{pmatrix} \tag{16}$$

$$C = \begin{pmatrix} \exp(iu) & 0 \\ 0 & \exp(-iu) \end{pmatrix}, \quad I = \begin{pmatrix} 1 & 0 \\ 0 & 1 \end{pmatrix}, \tag{17}$$

$\boldsymbol{u} := (u(x, t), u_t(x, t))$ is the potential and $\lambda \in \mathbb{C}$ denotes the spectral parameter.

The spectrum of $\mathscr{L}^{(x)}$ is defined as

$$\sigma(\mathscr{L}) := \{\lambda \in \mathbb{C} | \mathscr{L}^{(x)} \boldsymbol{v} = 0, |\boldsymbol{v}| \text{ bounded } \forall x\}. \tag{18}$$

Since the potential $\boldsymbol{u}$ solves the sine–Gordon equation and is of spatial period L, the spectrum is obtained using Floquet theory. The fundamental matrix, $M(x, x_0; \boldsymbol{u}, \lambda)$, of the spectral operator (15) is defined by

$$\mathscr{L}(\boldsymbol{u}, \lambda) M = 0, \quad M(x_0, x_0; \boldsymbol{u}, \lambda) = \begin{pmatrix} 1 & 0 \\ 0 & 1 \end{pmatrix}, \tag{19}$$

and the Floquet discriminant $\Delta(\boldsymbol{u}, \lambda) :=$ tr $M(x_0 + L, x_0; \boldsymbol{u}, \lambda)$. The spectrum of $\mathscr{L}(\boldsymbol{u}, \lambda)$ is given by the following condition on Δ:

$$\sigma(\mathscr{L}^{(x)}) := \{\lambda \in \mathbb{C} | \Delta(u, \lambda) \text{ is real and } -2 \leq \Delta(u, \lambda) \leq 2\}. \tag{20}$$

The discriminant is analytic in both its arguments. Moreover, for a fixed λ, Δ is invariant along solutions of the sine–Gordon equation:

$$\frac{d}{dt} \Delta(u(t), \lambda) = 0. \tag{21}$$

Since Δ is invariant and the functionals $\Delta(u, \lambda)$, $\Delta(u, \lambda')$ are pairwise in involution, Δ provides an infinite number of commuting invariants for the sine–Gordon equation.

When discussing the numerical experiments, we monitor the following elements of the spectrum which determine the nonlinear mode content of solutions of sine–Gordon equation and the dynamical stability of these modes:

(i) Simple periodic/antiperiodic spectrum

$$\sigma^s = \{\lambda_j^s | \Delta(\lambda, u) = \pm 2, d\Delta/d\lambda \neq 0\}.$$

(ii) Double points of the periodic/antiperiodic spectrum

$$\sigma^d = \{\lambda_j^d | \Delta(\lambda, u) = \pm 2, d\Delta/d\lambda = 0, d^2\Delta/d\lambda^2 \neq 0\}.$$

The periodic/antiperiodic or main spectrum provides the actions in an action-angle description of the system. The values of these actions fix a particular level set. Let λ denote the spectrum associated with the potential u. The level set defined by u is then given by

$$\mathscr{M}_u \equiv \{v \in \mathscr{F} | \Delta(v, \lambda) = \Delta(u, \lambda), \lambda \in \mathbb{C}\}. \tag{22}$$

Typically, $\mathscr{M}_u$ an infinite dimensional stable torus. However, the sine–Gordon phase space also contains degenerate tori which may be unstable. If a torus is unstable, its invariant level set consists of the torus and an orbit homoclinic to the torus. These invariant level sets, consisting of an unstable component, are represented in general by complex double points in the spectrum. A complete and detailed description of the sine–Gordon phase space structure is provided in [7]; we illustrate the main ideas by means of a simple example.

Consider the solution, $\boldsymbol{u}(x, t) = (\pi, 0)$. This solution is modulationally unstable: assuming that $u(x, t) = \pi + \varepsilon(x, t)$, $|\varepsilon(x, t)| \ll 1$, with $\varepsilon(x, t) = \hat{\varepsilon}_n(t) \exp(i\mu_n x) + \hat{\varepsilon}_n^*(t) \exp(-i\mu_n x)$, $\mu_n = 2\pi n/L$, n an arbitrary integer, it follows that

$$\frac{d^2}{dt^2} \hat{\varepsilon}_n + \omega_n^2 \hat{\varepsilon}_n = 0 \tag{23}$$

(and similarly for $\hat{\varepsilon}_n^*(t)$), where $\omega_n^2 = \mu_n^2 - 1$. The nth mode grows exponentially, if $0 \leq \mu_n^2 < 1$. For this solution, the Floquet discriminant is given by $\Lambda(\boldsymbol{u}, \lambda) = 2 \cos(\lambda + 1/16\lambda)L$ and the spectrum by $\sigma(\mathscr{L}) = \mathbb{R} \cup (|\lambda|^2 = \frac{1}{16})$. The periodic spectrum is located at $\lambda_j = \frac{1}{2}[j\pi/L \pm \sqrt{j^2\pi^2/L^2 - \frac{1}{4}}]$, j integer. Each of these points is a double point embedded in the continuous spectrum and becomes complex if $0 \leq (2\pi j/L)^2 < 1$. Note that the condition for complex double points is exactly the same as the condition for unstable modes.

The initial data used in the numerical experiments are small perturbations of $\boldsymbol{u}(x, t) = (\pi, 0)$. We begin by considering the case of two unstable modes. Figures 5 and 6 show three possible nearby states. Figure 5 is obtained using the

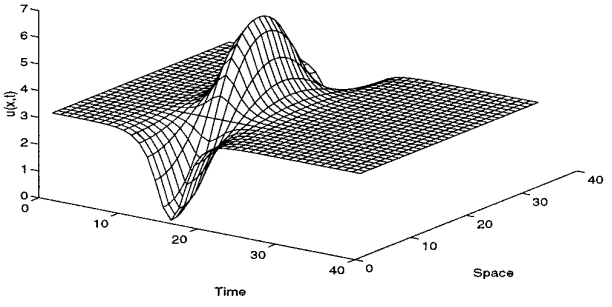

FIG. 5. The surface $u(x, t)$ of a homoclinic solution.

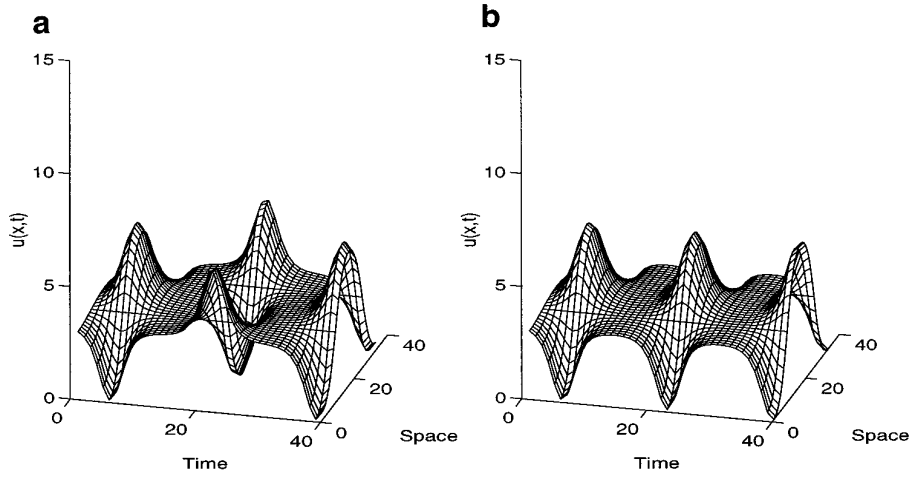

FIG. 6. (a) Outside the homoclinic orbit. (b) Inside the homoclinic orbit.

initial value,

$$u(x,0) = \pi + 0.1\cos(\mu x)$$
$$u_t(x,0) = 0.1\sqrt{1-\mu^2}\cos(\mu x),$$

where $L = 2\sqrt{2}\pi$ and $\mu = 2\pi/L$. It shows a solution homoclinic to $u_0(x,t) = \pi$. Figures 6a, b show solutions obtained using the initial values,

$$u(x,0) = \pi + 0.1\sqrt{1-\mu^2}\cos(\mu x)$$
$$u_t(x,0) = (0.1 \pm 0.01)\sqrt{1-\mu^2}\cos(\mu x).$$

Despite a small difference in the initial values, the subsequent behavior is quite different—the period shown in Fig. 6a is about twice that of Fig. 6b. We refer to these solutions as being "outside" and "inside" the homoclinic orbit, respectively. These differences are also reflected in the associated nonlinear spectrum and is shown in Fig. 7. Figure 7a corresponds to the homoclinic orbit of Fig. 5 and shows that both eigenvalues are double. Figures 7b, c, which are the spectral representations of the waveforms shown in Figs. 6a, b, respectively, show how the complex double point at 45° has split into two simple points; it has opened either into a "gap" in the spectrum (Fig. 7b) or has formed a "cross state" in the spectrum (Fig. 7c). These results were obtained analytically in [3] with a perturbation analysis.

Since the sine–Gordon equation is completely integrable, the main spectrum is invariant under the exact sine–Gordon flow. However, integrability is in general not preserved by numerical discretizations of the sine–Gordon equation and one finds that the main spectrum is not time-invariant under numerical flows. Said differently, the actions tend to drift under numerical flows. We are interested in the extent of this drift—the smaller the drift, the better the geometric structure of phase space is preserved. To answer the questions posed in the introduction regarding the effectiveness of symplectic integrators, in the numerical experiments we monitor the evolution of the main spectrum under the different numerical flows. This will provide a quantitative measure of the qualitative properties of symplectic and nonsymplectic discretizations of sine–Gordon.

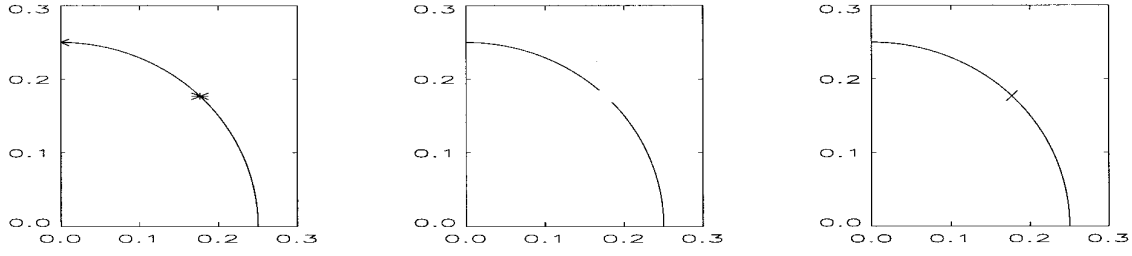

FIG. 7. The nonlinear spectrum: (a) Homoclinic orbit; (b) Inside the homoclinic orbit ("gap state"); (c) Outside the homoclinic orbit ("cross state").

4. NUMERICAL SCHEMES

The first thing we need to do in this section is to show how a finite-dimensional Hamiltonian system is obtained from the infinite-dimensional sine–Gordon system. The basic idea is to discretize the continuous Hamiltonian system (12). For example, if (12) is replaced by the following discrete analogue,

$$H = \sum_{j=0}^{N-1} \left[\tfrac{1}{2}\dot{\phi}_j^2 + \frac{1}{2h^2}(\phi_{j+1} - \phi_j)^2 + 1 - \cos\phi_j \right], \qquad \phi_{j+N} = \phi_j, \quad (24)$$

then Hamilton's equations,

$$\ddot{\phi}_j = -\frac{\partial H}{\partial \phi_j}, \quad \dot{\phi}_j = \frac{\partial H}{\partial \dot{\phi}_j},$$

lead to the standard second-order finite difference scheme,

$$\ddot{\phi}_j - \frac{1}{h^2}(\phi_{j-1} - 2\phi_j + \phi_{j+1}) + \sin\phi_j = 0. \quad (25)$$

However, if the continuous Hamiltonian (12) is replaced by

$$H = \tfrac{1}{2} \sum_{n=-N/2}^{(1/2)N-1} [|\dot{A}_n|^2 + \mu_n^2 |A_n|^2] - \frac{1}{N} \sum_{j=-N/2}^{(1/2)N-1} \cos\phi_j \quad (26)$$

the exponentially accurate (for analytic solutions) Fourier pseudospectral scheme,

$$\ddot{A}_n + \mu_n^2 A_n + F_n\{\sin\phi\} = 0, \quad (27)$$

is obtained, where

$$A_n = F_n\{\phi\} := \frac{1}{N} \sum_{j=-N/2}^{(1/2)N-1} \phi_j \exp(-2\pi i n j/N)$$

and

$$\phi_j = F_n^{-1}\{\boldsymbol{A}\} := \sum_{n=-N/2}^{(1/2)N-1} A_n \exp(2\pi i n j/N).$$

Thus, by discretizing the spatial variable, one reduces the infinite-dimensional sine–Gordon system to a finite-dimensional Hamiltonian system written in the form

$$\frac{dp_i}{dt} = -\frac{\partial H}{\partial q_i}, \quad \frac{dq_i}{dt} = \frac{\partial H}{\partial p_i}, \quad i = 1, ..., N, \quad (28)$$

or more conveniently as

$$\frac{d\boldsymbol{z}}{dt} = J^{-1}\mathbf{grad} H(\boldsymbol{z}), \quad (29)$$

where $\boldsymbol{z} := (\boldsymbol{p}, \boldsymbol{q})^{\mathrm{T}}$ and J is the so-called *symplectic matrix,*

$$J := \begin{pmatrix} 0_n & I_n \\ -I_n & 0_n \end{pmatrix} \quad (30)$$

with 0_n and I_n denoting the zero and unit matrices of dimension n, respectively.

Again, as in the planar case discussed in Section 2, we need to construct discretizations of (28) preserving its essential Hamiltonian nature. In the planar case, symplectic simply meant area preserving. The higher dimensional analogue is a little more complicated. If we denote the transformation from one time step to the next by ϕ (cf. (3)), the appropriate quantity to preserve for higher dimensional systems is given by

$$\phi'^{T} J \phi' = J \quad \forall (p, q) \in \Omega, \quad (31)$$

where ϕ' is the Jacobian matrix of the transformation and J is the (2×2)-dimensional symplectic matrix defined by (30). Again several procedures for constructing discretizations with exactly these properties have been developed. As in the planar case, one can ensure that the scheme is explicit if the Hamiltonian is separable, i.e., if

$$H(\boldsymbol{p}, \boldsymbol{q}) = T(\boldsymbol{p}) + V(\boldsymbol{q}).$$

Since the continuous Hamiltonian of the sine–Gordon equation is separable, its discretizations may inherit this property as demonstrated by (24) and (26), allowing for very efficient explicit implementations of the symplectic schemes.

In the next section we compare the higher dimensional counterparts of the first-, second-, and fourth-order symplectic discretizations defined by (6) with The Runge–Kutta methods of the same orders of accuracy.

5. NUMERICAL EXPERIMENTS

For the numerical experiments in the unstable regime, the initial data is used,

$$u(x, 0) = \pi + 0.1\cos(\mu x), \quad u_t(x, 0) = 0, \quad (32)$$

with parameters $\mu = 2\pi/L$ and $L = 2\sqrt{2}\pi$. This initial data is in the "effectively" chaotic regime as the zeroth double point remains closed; i.e., the initial data is on the level set containing the homoclinic manifold. Closed double points

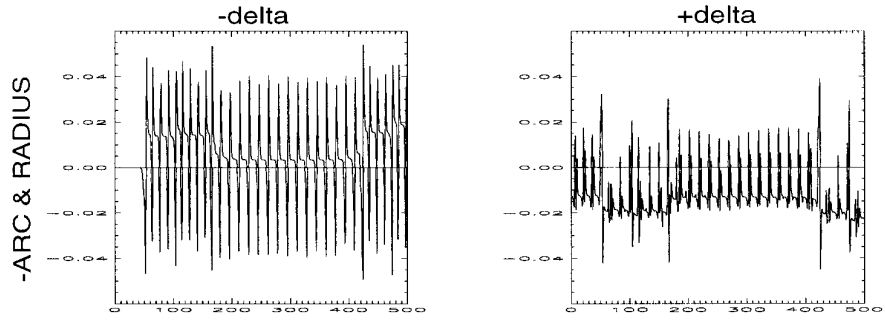

FIG. 8. fd1sy: $u(x, 0) = \pi + 0.1 \cos \mu x$, $u_t(x, 0) = 0$, $N = 64$, $t = 0 - 500$.

cannot be preserved by the numerical schemes and in the following experiments one observes that the zeroth mode is immediately split into a gap state by the numerical scheme.

To interpret the evolution of spectrum plots, recall that under perturbations the complex double points can split in two ways—either into a gap along an arc of the circle, or into a cross along the radius (cf. Fig. 7). For each set of experiments, we show a signed measure of the splitting distance for each complex double point as a function of time. Positive and negative values represent gap and cross states, respectively. Homoclinic crossings occur when the splitting distance passes through zero.

We begin by examining the finite difference scheme (25) implemented with Runge–Kutta (second and fourth order) and symplectic (first, second, and fourth order) integrators. These schemes are denoted FD2RK, FD4RK and FD1SY, FD2SY, FD4SY, respectively. We use $N = 64$ and a fixed time step $\Delta t = L/512$ in the finite difference experiments. The evolution of the spectrum associated with the first two nonlinear modes under the FD1SY, FD2RK, FD2SY, FD4RK, FD4SY flows are given in Figs. 8–12. Note that we measure the nonlinear spectrum throughout with an accuracy of about 10^{-6}.

For FD1SY, a chaotic flipping between gap and cross states for both the zeroth and first modes is observed (Fig. 8) and the magnitude of the spectral deviation is of the order of 4×10^{-2}. Using second-order time integrators, FD2RK (Fig. 9) and FD2SY (Fig. 10), the zeroth and first modes execute a few homoclinic crossings before drifting into cross and gap states, respectively, indicating that the solution has collapsed onto a nearby (stable) periodic orbit. The spectral deviations have diminished in magnitude to the order of 2×10^{-2}. Using the fourth-order integrators, FD4RK (Fig. 11) and FD4SY (Fig. 12), the zeroth mode does not execute any homoclinic crossings and immediately collapses into a gap state. No further improvement in the preservation of the spectrum is detected since, for these schemes, the perturbation due to the spatial truncation dominates that of the temporal truncation. In the finite difference experiments, large deviations in the spectrum occur, regardless of whether the integrator is symplectic or not. The finite-difference scheme performs quite poorly; it does not preserve either component of the spectral configuration. More importantly, there is *no* substantial difference in the performance of the Runge–Kutta and symplectic integrators.

One might argue that the similarities between the symplectic and nonsymplectic schemes are due to an inadequate spatial resolution provided by the finite difference spatial discretization. Accordingly, we now consider the exponentially accurate Fourier pseudospectral method (27) implemented with Runge–Kutta (second and fourth order) and symplectic (first, second, and fourth order) integrators. These schemes are denoted by PS2RK, PS4RK and PS1SY, PS2SY, PS4SY, respectively. In the pseudospectral experiments we use $N = 32$ Fourier modes and a

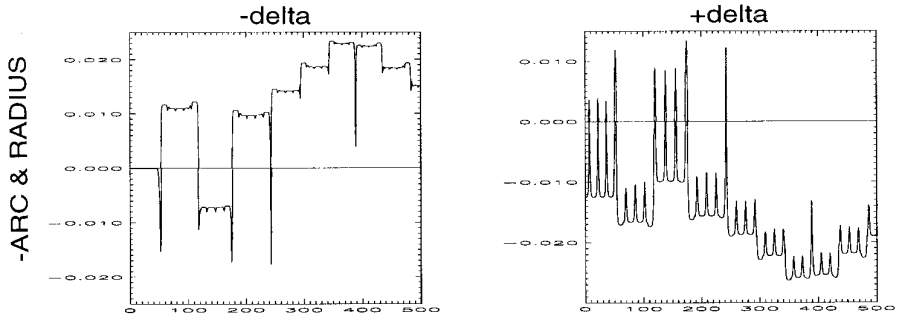

FIG. 9. fd2rk: $u(x, 0) = \pi + 0.1 \cos \mu x$, $u_t(x, 0) = 0$, $N = 64$, $t = 0 - 500$.

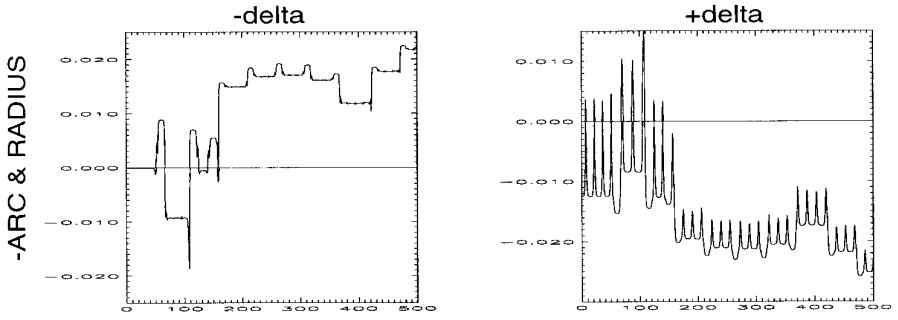

FIG. 10. fd2sy: $u(x, 0) = \pi + 0.1 \cos \mu x$, $u_t(x, 0) = 0$, $N = 64$, $t = 0 - 500$.

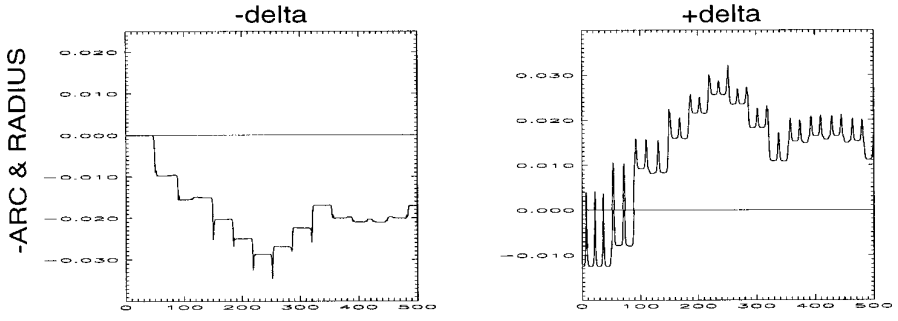

FIG. 11. fd4rk: $u(x, 0) = \pi + 0.1 \cos \mu x$, $u_t(x, 0) = 0$, $N = 64$, $t = 0 - 500$.

fixed time step, $\Delta t = L/512$. For initial data (17), the deviations in the spectrum corresponding to the first two nonlinear modes under the PSISY, PS2RK, PS2SY, PS4RK, PS4SY flows are given in Figs. 13–17 for $0 \le t \le 500$. This method is exponentially accurate in space, which allows for a very accurate initial approximation of the spectral configuration. The evolution of the spectrum under the numerical flow is primarily due to the time integrators.

The splitting distance for both modes obtained with PS1SY (Fig. 13) is $O(10^{-2})$ (i.e., it is comparable to the splitting distance obtained with FD1SY) and is larger than that obtained with the Runge–Kutta schemes. This result highlights the fact that symplecticness is not enough to preserve the phase space geometry.

The pseudospectral method does provide substantial improvement over the finite difference discretization. Using PS2RK (Fig. 14) and PS2SY (Fig. 15), the spectrum for the first mode does not execute any homoclinic crossings and so the torus component is much more accurately preserved than with the previous spatial discretizations. The zeroth mode still displays homoclinic crossings which occur earlier than with the lower order PS1SY. Since the initial data is chosen on the homoclinic manifold, it is to be expected that there will be an earlier onset and higher

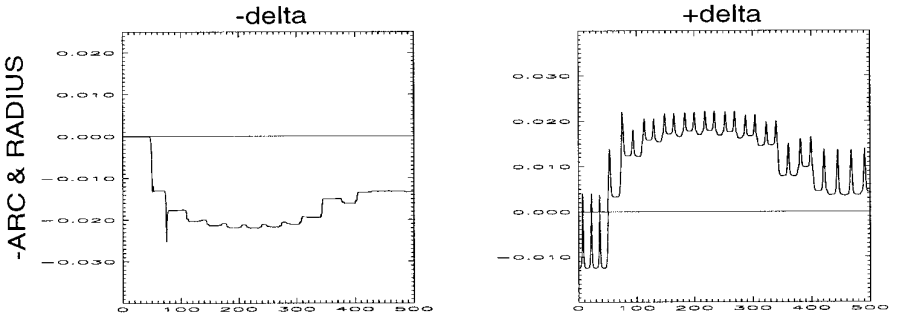

FIG. 12. fd4sy: $u(x, 0) = \pi + 0.1 \cos \mu x$, $u_t(x, 0) = 0$, $N = 64$, $t = 0 - 500$.

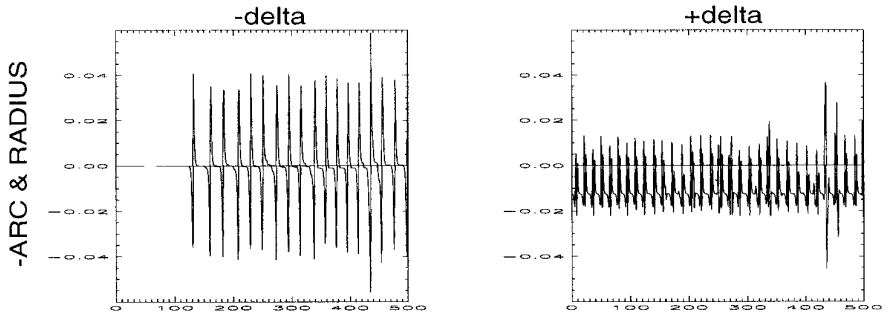

FIG. 13. ps1sy: $u(x, 0) = \pi + 0.1 \cos \mu x$, $u_t(x, 0) = 0$, $N = 32$, $t = 0 - 500$.

density of homoclinic crossings when a more accurate scheme is used. Refinement can accentuate the frequency of homoclinic crossings as the numerical trajectory is trapped in a narrower band about the homoclinic manifold. With PS2RK there is a $O(10^{-3})$ drift in the zeroth mode, but no strong growth. The drift is eliminated when using PS4RK (Fig. 16). The spectral deviations are $O(10^{-4})$ for PS4RK and PS4SY (Fig. 17). Again, there is *not* an appreciable difference between the Runge–Kutta and symplectic integrators in their ability to preserve the integrable structure. An accurate representation of the global structures appears to be more a function of accuracy than symplecticness. In this effectively chaotic region of phase space, the chaotic width about the unstable torus is only slightly more sharply defined with the symplectic integrator.

In long time studies of low-dimensional Hamiltonian systems, symplectic integrators have been reported as superior in capturing global phase space structures since standard integrators may allow the actions to drift [17]. To investigate this issue for sine–Gordon, we examine a time slice $10{,}000 \leq t \leq 10{,}500$. For PS4RK (Fig. 18) the deviations in the actions associated with the zeroth mode oscillates about 1.2×10^{-4}, whereas for PS4SY (Fig. 19) it oscillates about 5×10^{-5}. However, the Runge–Kutta integrator can be made more efficient using variable time steps. We apply the Runge–Kutta code, D02DDf, of the

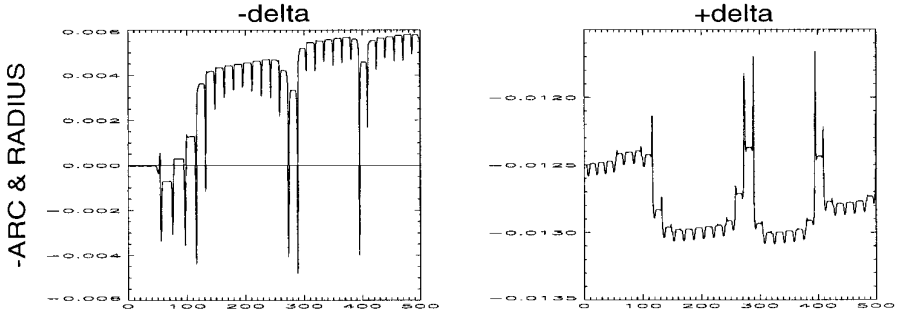

FIG. 14. ps2rk: $u(x, 0) = \pi + 0.1 \cos \mu x$, $u_t(x, 0) = 0$, $N = 32$, $t = 0 - 500$.

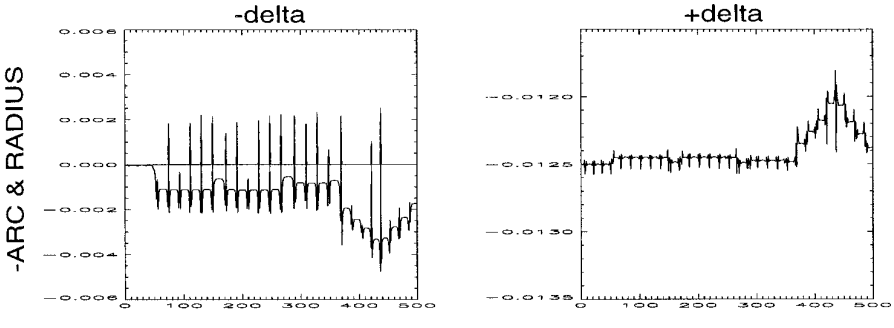

FIG. 15. ps2sy: $u(x, 0) = \pi + 0.1 \cos \mu x$, $u_t(x, 0) = 0$, $N = 32$, $t = 0 - 500$.

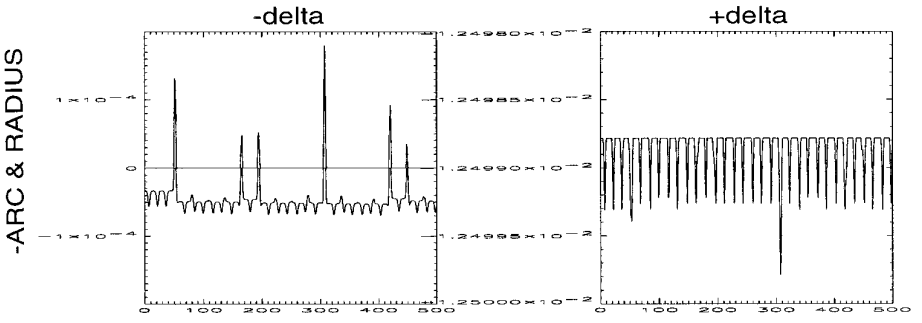

FIG. 16. ps4rk: $u(x, 0) = \pi + 0.1 \cos \mu x$, $u_t(x, 0) = 0$, $N = 32$, $t = 0 - 500$.

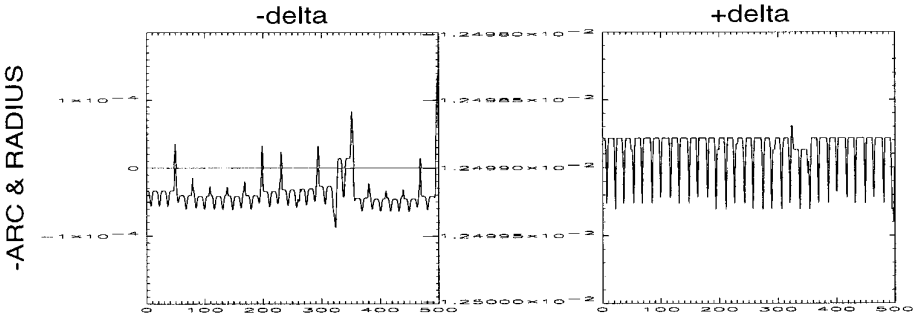

FIG. 17. ps4sy: $u(x, 0) = \pi + 0.1 \cos \mu x$, $u_t(x, 0) = 0$, $N = 32$, $t = 0 - 500$.

NAG library which is a fully adaptive time stepping method, to the pseudospectral method (PSNAG). PSNAG (Fig. 20) does provide an improvement as it oscillates about 5×10^{-5}. The chaotic width (amplitude of the splitting distance) obtained with the fixed time step has been diminished with this adaptive method. Consequently, for the long timescale regime, the slight advantage obtained with PS4SY has been eliminated using variable time steps.

To determine if an improvement in the performance of symplectic integrators occurs when dealing with stable structures, we have used the initial data

$$u_0 = 3.1 + 0.1(\cos(\mu x) + \cos(2\mu x)), \quad L = 4\sqrt{2}\pi, \quad (33)$$

which is a finite distance away from the homoclinic manifold. Initially we are nearby a solution ($u = \pi$) with three unstable modes—however, all the double points have been split into gaps of magnitude 10^{-2} by the *initial* values and we refer to this as the stable case. In order to obtain homoclinic crossings, the perturbations in the λ need to be more than 10^{-2}. Therefore, provided the numerical schemes are sufficiently accurate, no homoclinic crossings are expected. Although the results are not presented here, we note that our studies in this regime confirm our previous observations: the first order symplectic scheme executes deviations large enough for homoclinic crossings to occur. A comparison of the second- and fourth-order symplectic

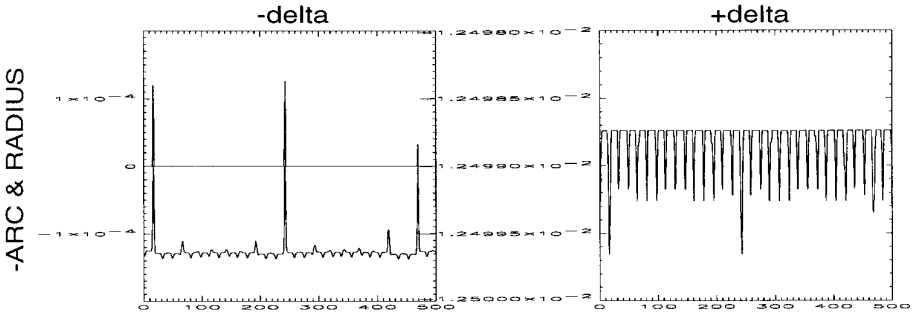

FIG. 18. ps4rk: $u(x, 0) = \pi + 0.1 \cos \mu x$, $u_t(x, 0) = 0$, $N = 32$, $t = 10000 - 10500$.

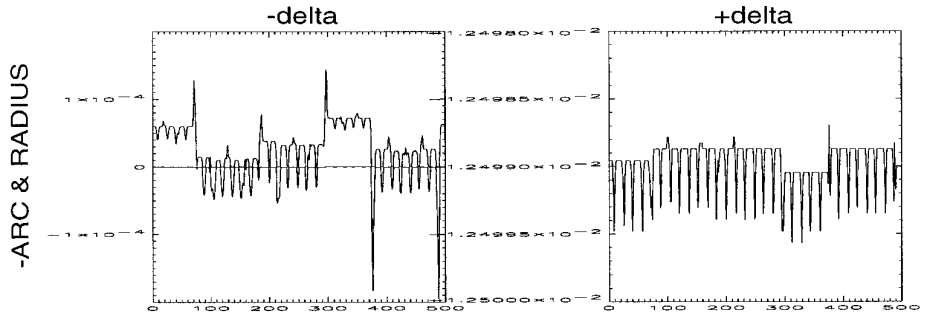

FIG. 19. ps4sy: $u(x, 0) = \pi + 0.1 \cos \mu x$, $u_t(x, 0) = 0$, $N = 32$, $t = 10000 - 10500$.

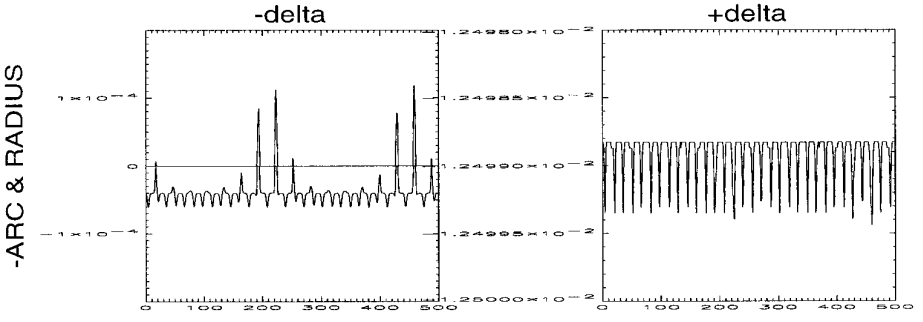

FIG. 20. psnag: $u(x, 0) = \pi + 0.1 \cos \mu x$, $u_t(x, 0) = 0$, $N = 32$, $t = 10000 - 10500$.

and Runge–Kutta schemes shows that the symplectic schemes capture most of the phase space structures of interest, although not substantially more accurately than the standard schemes which do not take into account the Hamiltonian nature. In fact, a drift in the actions occurs even when using the symplectic integrators and is eliminated using a smaller time step.

6. CONCLUSIONS

In this investigation of numerical solutions of the sine–Gordon equation, the nonlinear spectral decomposition of the solution provides considerable insight into the behavior of the various schemes. For the finite difference method, interesting lattice dynamics such as collapsing effects occur, but as a numerical scheme it performs poorly. The pseudospectral method with a high order integrator (*regardless of type*) produced the smallest deviations in the actions and best represented the qualitative properties of the equation. Using the same fixed time step in the symplectic and standard integrators, we have *not* found an appreciable (i.e., an order of magnitude) difference in their ability to preserve the phase space structure. It appears to depend more upon the accuracy of the numerical scheme rather than the property of symplecticness. Smaller step sizes were not necessary for the standard integrators to capture the same features as those obtained with the symplectic integrators. In addition, the Runge–Kutta integrators we employ are not state of the art. If a sophisticated variable time step method is used, the very small improvement seen using the symplectic method may be lost. Even for long time integrations, where symplectic integrators perform better in low dimensional problems because the standard schemes sometimes permit a drift in the actions, no significant difference was detected, either in the stable or the unstable regimes. Consequently, there does not appear to be a clear advantage in using symplectic integrators for numerical implementation of the sine–Gordon equation.

Although we have been examining a specific integrable equation, we believe the results are extendable to other infinite-dimensional Hamiltonian systems (e.g., the nonlinear Schrodinger equation) which share a similar phase space structure.

ACKNOWLEDGMENTS

This work was partially supported by AFOSR grant F49620-94-0120, ONR Grant N00014-94-0194, and NSF Grants DMS-9024528, DMS-9404265. We thank Ed Overman for the use of his spectral solver for the sine–Gordon equation.

REFERENCES

1. M. J. Ablowitz and H. Segur, *Solitons and the Inverse Scattering Transform* (SIAM, Philadelphia, 1981).

2. M. J. Ablowitz and B. M. Herbst, On homoclinic structure and numerically induced chaos for the nonlinear Schrödinger equation, *SIAM J. Appl. Math.* **50,** 339 (1990).
3. M. J. Ablowitz, B. M. Herbst, and C. M. Schober, *On the Numerical Solution of the Sine–Gordon Equation. I. Integrable Discretizations and Homoclinic Manifolds,* Program in Applied Mathematics Report PAM #214, University of Colorado, 1995.
4. M. J. Ablowitz, B. M. Herbst, and C. M. Schober. On the numerics of integrable discretizations, preprint.
5. V. I. Arnold, *Mathematical Methods of Classical Mechanics* (Springer-Verlag, New York, 1978).
6. A Bobenko and U. Pinkall, Discrete surfaces with constant negative curvature, SFB 288, Preprint No. 127, Berlin, 1994.
7. N. Ercolani, M. G. Forest, and D. W. McLaughlin, Geometry of the modulational instability. Part III. Homoclinic orbits for the periodic sine–Gordon equation, *Physica D* **43,** 349 (1990).
8. L. D. Faddeev and L. A. Takhtajan, *Hamiltonian Methods in the Theory of Solitons* (Springer-Verlag, Berlin, 1987).
9. B. M. Herbst and M. J. Ablowitz, Numerically induced chaos in the nonlinear Schrödinger equation, *Phys. Rev. Lett.* **62,** 2065 (1989).
10. B. M. Herbst and M. J. Ablowitz, Numerical homoclinic instabilities in the sine–Gordon equation, *Quaestiones Math.* **15,** 345 (1992).
11. B. M. Herbst and M. J. Ablowitz, Numerical chaos, symplectic integrators and exponentially small splitting distances, *J. Comput. Phys.* **105,** 122 (1993).
12. B. M. Herbst, G. J. le Roux, and M. J. Ablowitz, Chaos in numerics, preprint.
13. R. Hirota, Nonlinear partial difference equations III; Discrete sine–Gordon equation, *J. Phys. Soc. Japan* **43,** 2079 (1977).
14. V. F. Lazutkin, Analytic integrals of the semistandard map, and splitting of separatrices, *Leningrad Math. J.* **1,** 427 (1990).
15. V. F. Lazutkin, On the width of the instability zone near the separatrix of a standard map, *Soviet Math. Dokl.* **42,** 5 (1991).
16. V. F. Lazutkin, I. G. Schachmannski, and M. B. Tabanov, Splitting of separatrices for standard and semistandard mappings, *Physica D* **40,** 235 (1989).
17. J. M. Sanz-Serna and M. P. Calvo, *Numerical Hamiltonian Problems* (Chapman & Hall, London, 1994).
18. M. J. Ablowitz, C. M. Schober, and B. M. Herbst, Numerical chaos, roundoff errors and homoclinic orbits, *Phys. Rev. Lett.* **71,** 2683 (1993).
19. H. Yoshida, Construction of higher order symplectic integrators, *Phys. A.* **150,** 262 (1990).